STABILITY ANALYSIS OF PERTURBED PLANE COUETTE FLOW

Dwight Barkley

Mathematics Institute,

University of Warwick, Coventry, CV4 7AL, United Kingdom

barkley@maths.warwick.ac.uk

Laurette S. Tuckerman

LIMSI-CNRS, BP 133, 91403 Orsay Cedex, France

laurette@limsi.fr

(February 6, 1998)

Abstract

Plane Couette flow perturbed by a spanwise oriented ribbon, similar to a configuration investigated experimentally at CEA-Saclay, is investigated numerically using a spectral-element code. 2D steady states are computed for the perturbed configuration; these differ from the unperturbed flows mainly by a region of counter-circulation surrounding the ribbon. The 2D steady flow loses stability to 3D eigenmodes at $Re_c = 230, \beta_c = 1.3$ for $\rho = 0.086$ and $Re_c \approx 550, \beta_c \approx 1.5$ for $\rho = 0.043$, where β is the spanwise wavenumber and 2ρ is the width of the ribbon. The bifurcation is determined to be subcritical by calculating the cubic term in the normal form equation from the time-series of a single nonlinear simulation. The critical eigenmode and nonlinear 3D states contain streamwise vortices localized in the streamwise direction. The streamwise extent of the vortices in the nonlinear state decreases with decreasing Re. All of these results agree well with experimental observations.

I. INTRODUCTION

It is well known that, of the three shear flows most commonly used to model transition to turbulence, plane Poiseuille flow is linearly unstable for $Re > 5772$, whereas plane Couette flow and pipe Poiseuille flow are linearly stable for all Reynolds numbers; see, e.g. [1]. Yet, as is also well established, in laboratory experiments all three flows actually undergo transition to three-dimensional turbulence for Reynolds numbers on the order of 300 for plane Couette flow and on the order of 1000 for plane and pipe Poiseuille flows.

The gap between steady, linearly stable flows which depend on only one spatial coordinate and three-dimensional turbulence can be bridged by studying perturbed versions of Couette and Poiseuille flow. Plane Couette flow perturbed by a wire midway between the bounding plates and oriented in the spanwise direction has been the subject of laboratory experiments by Dauchot and co-workers [2–4] at CEA-Saclay. Our goal in this paper is to study numerically the flows and transitions in a configuration similar to that of the Saclay experiments.

Previous studies of plane channel flows have used a variety of approaches. We briefly review these, emphasizing computational investigations and the plane Couette case.

One approach is to seek finite amplitude solutions at transition Reynolds numbers and to understand the dynamics of transition in terms of these solutions. Finite amplitude solutions for plane Couette flow have been found for Reynolds numbers as low as $Re = 125$ by numerically continuing steady states or travelling waves from other flows: the wavy Taylor vortices of cylindrical Taylor-Couette flow by Nagata [5] and Conley and Keller [6] and the wavy rolls of Rayleigh-Bénard convection by Busse [7]. Most recently, Cherhabili and Ehrenstein [8,9] succeeded in continuing plane-Poiseuille-flow solutions to plane Couette flow, via an intermediate Poiseuille-Couette family of flows. They showed that in proceeding from Poiseuille to Couette flow, the wavespeed of the travelling waves decreases and their streamwise wavelength increases, as does the number of harmonics needed to capture them. When the Couette limit is reached, the finite amplitude solutions are highly localized steady

states. The minimum Reynolds number achieved in these continuations is $Re = 1500$.

A second, highly successful, approach has been to study the transient evolution of linearized plane Couette flow. Although all initial conditions must eventually decay and the most slowly decaying mode must be spanwise invariant by Squire's theorem, the non-normality of the evolution operator allows large transient growth. Butler and Farrell [10] showed that a thousand-fold growth in energy could be achieved from an initial condition resembling streamwise vortices which are approximately circular and streamwise invariant. Reddy and Henningson [11] computed the maximum achievable growth for a large range of Reynolds numbers. An interpretation is given by these authors and by Trefethen et al. [12] in terms of pseudospectra: the spectra of non-normal operators display an extreme sensitivity to perturbations of the operator. Thus, slightly perturbed plane Couette or Poiseuille flows may be linearly unstable for much lower Reynolds numbers than the unperturbed versions.

A third broad category of computational investigation is the study of nonlinear temporal evolution in relatively tame turbulent plane channel flows. Orszag and Kells [13] and Orszag and Patera [14] showed that finite amplitude spanwise-invariant states of plane Poiseuille flow are unstable to 3D perturbations; this is also true of quasi-equilibria for plane Poiseuille and Couette flow. Numerical simulations by Hamilton, Kim and Waleffe [15] of low Reynolds number turbulence in plane Couette flow indicated that streamwise vortices and streaks played an important role in a quasi-cyclic regeneration process. Coughlin [16] used weak forcing to stabilize steady states containing streamwise vortices and streaks. These became unstable and underwent a similar regeneration cycle when the forcing or Reynolds number was increased.

The last approach we discuss, and the most relevant to this study, is perturbation of the basic shear profile, in order to elicit instabilities that are in some sense nearby. If a geometric perturbation breaks either the streamwise or spanwise invariance of the basic profile, then the flow is freed from the constraint of Squire's theorem, which would otherwise imply that the linear instability at lowest Reynolds number is to a spanwise invariant (2D) eigenmode. A perturbed flow with broken symmetry may directly undergo a 3D linear instability. One

can hope to understand the behavior of the unperturbed system by considering the limit in which the perturbation goes to zero. For some time, experimentalists [17] have used perturbations to produce spanwise-invariant Tollmien-Schlichting waves arising subcritically. More recently, for example, Schatz et al. [18] inserted a periodic array of cylinders in a plane Poiseuille experiment to render this bifurcation supercritical. In plane Couette flow, Dauchot and co-workers at Saclay [2–4] found that streamwise vortices could be induced for Reynolds numbers around 200 when a wire was placed in the flow (the exact range in Reynolds number for which the vortices occur depends on the radius of the wire). They suspected that these vortices arise from a subcritical bifurcation from the perturbed profile, but did not determine this.

In this paper, we numerically study the destabilization of plane Couette flow when a ribbon is placed midway in the channel gap (Fig. 1). The ribbon is infinitely thin in the streamwise (x) direction, has height 2ρ in the cross-channel (y) direction, and is infinite in the spanwise (z) direction. This geometry is similar, though not identical, to that used in the Saclay experiments. In the experiments, the perturbation is a thin wire with cylindrical cross-section. Here we use a ribbon because it is much easier to simulate numerically.

We shall address the extent to which a small geometric perturbation of the plane Couette geometry affects the stability of the flow. We will show that a small geometric perturbation does indeed lead to a subcritical bifurcation to streamwise vortices, at Reynolds numbers and wavenumbers which agree well with the Saclay experiments.

FIGURES

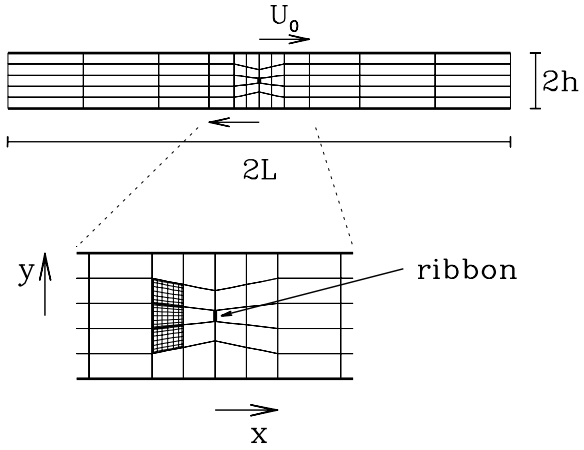

FIG. 1. Flow geometry considered in the paper. The upper and lower channel walls are separated by distance $2h$ and move with velocities $U_0\hat{x}$ and $-U_0\hat{x}$, repectively. An infinitely thin ribbon (bold line) is located midgap in the channel and has height 2ρ ($\rho/h = 0.086$ for the case shown). The computational mesh (macro elements) used in our calculations is shown, as is the (fine) collocation mesh for polynomial order $N = 8$ (three elements in the enlargement). The ribbon is formed by setting no-slip boundary conditions on the edges of two adjoining elements. Periodic boundary conditions are imposed over length $2L$ in the horizontal direction. The full geometry shown has aspect ratio $L/h = 10$. The system is homogeneous in the spanwise (z)-direction normal to the figure.

II. NUMERICAL COMPUTATIONS

The computations consist of three parts: (1) obtaining steady 2D solutions of the Navier–Stokes equations, (2) determining the linear stability of these solutions to 3D perturbations, and (3) classifying the bifurcation via a nonlinear stability analysis. Here we outline the numerical techniques for carrying out these computations.

A. 2D steady flows

Our computational domain has been shown in fig. 1. We non-dimensionalize lengths by the channel half-height h, velocities by the speed U_0 of the upper channel wall, time by the convective time h/U_0. There are two nondimensional parameters for the flow, which we take to be the usual Reynolds number for plane Couette flow, $Re = hU_0/\nu$, where ν is the kinematic viscosity of the fluid, and the nondimensional half-height of the ribbon ρ, hereafter called its radius for consistency with the Saclay experiments. We view the (nondimensionalized) streamwise periodicity length $2L$ as a numerical parameter which we take sufficiently large that the system behaves as though it were infinite in the streamwise direction.

The fluid flow is governed by the incompressible Navier–Stokes equations:

$$\frac{\partial \mathbf{u}}{\partial t} = -(\mathbf{u}\cdot\nabla)\mathbf{u} - \nabla p + \frac{1}{Re}\nabla^2\mathbf{u} \quad \text{in } \Omega, \tag{1a}$$

$$\nabla\cdot\mathbf{u} = 0 \quad \text{in } \Omega, \tag{1b}$$

subject to the boundary conditions:

$$\mathbf{u}(x-L,y) = \mathbf{u}(x+L,y) \tag{2a}$$

$$\mathbf{u}(x,y=\pm 1) = \pm\hat{\mathbf{x}} \tag{2b}$$

$$\mathbf{u}(x=0,y) = 0, \qquad \text{for } -\rho \le y \le \rho, \tag{2c}$$

where $\mathbf{u} \equiv (u,v,w)$ is the velocity field, p is the nondimensionalized static pressure and Ω is the computational domain. The pressure p, like $\mathbf{u}$, satisfies periodic boundary conditions in x.

Time-dependent simulations of these equations in two dimensions ($w \equiv 0$, $\partial/\partial z \equiv 0$) are carried out using the spectral element [19] program *Prism* [20,21]. In the spectral element method, the domain is represented by a mesh of macro elements as shown in Fig. 1. The channel height is spanned by five elements while the number of elements spanning the streamwise direction depends on its length: 24 elements are used for $L = 32$ and

36 elements for $L = 56$. The no-slip condition (2c) is enforced by setting zero velocity boundary conditions along the edges of two adjoining mesh elements: this interface defines the ribbon. If continuity were imposed along this interface, as is normally done, then the flow would reduce to unperturbed plane Couette flow. Thus the ribbon is modeled by a small (but significant) change in the boundary conditions on just two edges of elements in the computational domain. Within each element both the geometry and the solution variables (velocity and pressure) are represented using Nth order tensor-product polynomial expansions. The collocation mesh in Fig. 1 (enlargement) corresponds to an expansion with $N = 8$.

A time-splitting scheme is used to integrate the underlying discretized equations [22]. Based on simulations with polynomial order N in the range $6 \leq N \leq 12$ and timesteps $\triangle t$ in the range $10^{-3} \leq \triangle t \leq 10^{-2}$ we have determined that $N = 8$ and $\triangle t = 0.005$ give valid results over the range of Re considered. These numerical parameter values (typical for studies of this type) have been used for most of the results reported. Each velocity component is thus represented by about 7500 scalars.

Steady flows used for our stability calculations have been obtained from simulations with Reynolds numbers in the range $100 \leq Re \leq 600$. In all cases, the simulations were run sufficiently long to obtain asymptotic, steady velocity fields. We shall denote these steady 2D flows by $\mathbf{U}(x, y)$.

B. Linear stability analysis

Let $\mathbf{U}(x, y)$ be the 2D base flow whose stability is sought. An infinitesimal three-dimensional perturbation $\mathbf{u}'(x, y, z, t)$ evolves according to the Navier–Stokes equations linearized about $\mathbf{U}$. Because the resulting linear system is homogeneous in the spanwise direction z, generic perturbations can be decomposed into Fourier modes with spanwise wavenumbers β:

$$\begin{aligned} \mathbf{u}'(x,y,z,t) &= (\hat{u}\cos\beta z,\ \hat{v}\cos\beta z,\ \hat{w}\sin\beta z) \\ p'(x,y,z,t) &= \hat{p}\cos\beta z \end{aligned} \tag{3}$$

or an equivalent form obtained by translation in z. The vector $\hat{\mathbf{u}}(x,y,t) = (\hat{u},\hat{v},\hat{w})$ of Fourier coefficients evolves according to:

$$\frac{\partial\hat{\mathbf{u}}}{\partial t} = -(\hat{\mathbf{u}}\cdot\nabla)\mathbf{U} - (\mathbf{U}\cdot\nabla)\hat{\mathbf{u}} - (\nabla - \beta\hat{\mathbf{z}})\hat{p} + \frac{1}{Re}(\nabla^2 - \beta^2)\hat{\mathbf{u}} \quad \text{in } \Omega, \tag{4a}$$

$$(\nabla + \beta\hat{\mathbf{z}})\cdot\hat{\mathbf{u}} = 0 \qquad \text{in } \Omega, \tag{4b}$$

where ∇, etc. are two-dimensional differential operators. Equations (4) are solved subject to homogeneous boundary conditions:

$$\hat{\mathbf{u}}(x-L,y) = \hat{\mathbf{u}}(x+L,y) \tag{5a}$$

$$\hat{\mathbf{u}}(x,y=\pm 1) = 0 \tag{5b}$$

$$\hat{\mathbf{u}}(x=0,y) = 0, \qquad \text{for } -\rho \le y \le \rho, \tag{5c}$$

Equations (4) with boundary conditions (5) can be integrated numerically by the method described in section II A. For fixed β, this is essentially a two-dimensional calculation [23,24]. After integrating (4)-(5) a sufficiently long time, only eigenmodes corresponding to leading eigenvalues remain. We use this to find the leading eigenvalues (those with largest real part) and corresponding eigenmodes for fixed values of Re and β as follows. A Krylov space is constructed based on integrating (4)-(5) over $K = 8$ successive (dimensionless) time intervals of $T = 5$. Approximate eigenvalues σ and eigenmodes $\tilde{\mathbf{u}}(x,y,z)$ are calculated; their accuracy is tested by computing the residual $r \equiv ||\sigma\tilde{\mathbf{u}} - \mathbf{L}\tilde{\mathbf{u}}||$, where $\mathbf{L}\tilde{\mathbf{u}}$ is the right-hand-side of the linearized Navier-Stokes equations. If the eigenvalue-eigenmode pairs do not attain a desired accuracy ($r < 10^{-5}$ for the case here), then another iteration is performed. The new vector is added to the Krylov space and the oldest vector is discarded. This is effectively subspace iteration initiated with a Krylov subspace. More details can be found in [18,23,25].

We conclude this section by considering the effect of the streamwise periodicity length $2L$ on the computations. Recall that we view L as a quasi-numerical parameter in that we

seek solutions valid for large L. Figure 2 shows the dependence of the leading eigenvalue σ on streamwise length at $Re = 250$, $\beta = 1.3$ (values near the primary 3D linear instability). It can be seen that for $L \gtrsim 32$ the eigenvalue is independent of L. This is consistent with the structure of the base flow and eigenmodes shown in the following section. Most of the computations reported have used $L = 32$.

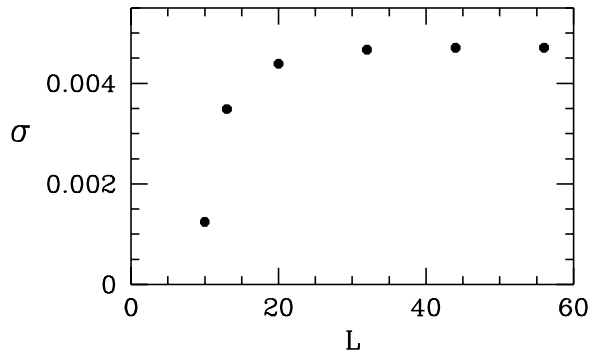

FIG. 2. Leading eigenvalue as a function of streamwise periodicity half-length L for $Re = 250$, $\beta = 1.3$. For $L \gtrsim 32$ the eigenvalue is independent of L.

C. 3D simulations

For the nonlinear stability analysis, we carry out 3D simulations of (1)-(2) using the same spectral element representation in (x, y) described above together with a Fourier representation in the spanwise direction z. We impose periodicity in the spanwise direction by including wavenumbers $m\beta_c$ for integers $|m| < M/2$, where β_c is the critical wavenumber found in the linear stability analysis. We find that $M = 16$ is sufficient to resolve the flow over the time of our simulation.

III. RESULTS

A. Steady flows

A typical steady 2D flow for the perturbed Couette geometry is shown in Fig. 3. It is representative of base flows for Reynolds numbers on the order of a few hundred with a ribbon of size $\rho = 0.086$. This was chosen to correspond to the radius of one of the cylinders used in the Saclay experiments [2–4]. The Reynolds number $Re = 250$ of the flow shown is close to the threshold for the 3D instability that will be discussed in the next section. Unless otherwise stated, all results are for $\rho = 0.086$, $Re = 250$, and $L = 32$.

In Fig. 3(a) it can been seen that, except near the ribbon, the steady flow is essentially the parallel shear of unperturbed plane Couette flow. The streamlines are as reported experimentally in [2]. As noted there, the Reynolds number based on the length of the ribbon and the local velocity near the ribbon is very small compared to Reynolds numbers where separation or vortex shedding could be expected. In Fig. 3(b) we plot the streamfunction of the deviation $\mathbf{U} - \mathbf{U}_C$ where $\mathbf{U}_C = y\hat{\mathbf{x}}$ is the unperturbed plane Couette profile. The primary effect of the ribbon is to establish a region ($|x| \lesssim 3$) of positive circulation (opposing that of plane Couette flow) surrounding the ribbon. Figure 3(c) shows $\mathbf{U} - \mathbf{U}_C$ over a larger streamwise extent. Further from the ribbon are wider regions ($3 \lesssim |x| \lesssim 24$) in which the deviation is weak, but has the same positive circulation as plane Couette flow.

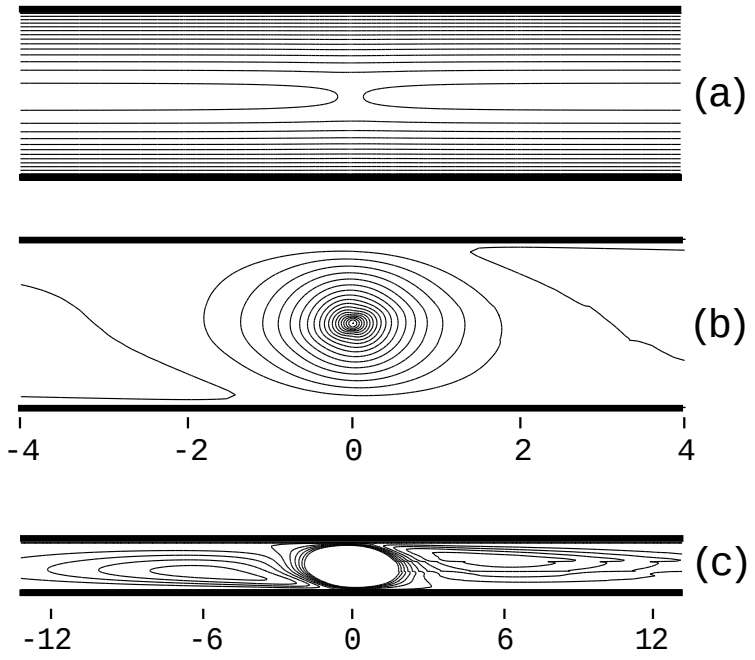

FIG. 3. The steady two-dimensional base flow $\mathbf{U}(x,y)$ at $Re = 250$ for a ribbon with $\rho = 0.086$. Only the central portion of the full $L = 32$ domain is shown. (a) Streamfunction contours of $\mathbf{U}$. The flow is nearly identical to the parallel shear of plane Couette flow except very near the ribbon. (b) Streamfunction contours of the deviation $\mathbf{U} - \mathbf{U}_C$ highlighting the difference between the perturbed and unperturbed Couette flows. A region ($|x| \lesssim 3$) of positive circulation is established around the ribbon. The flow is centro-symmetric. (c) The deviation over a larger streamwise extent showing regions ($3 \lesssim |x| \lesssim 24$) further from the ribbon whose circulation is negative, like that of $\mathbf{U}_C$. The flow is very weak; contours of the dominant part of this flow are not shown. The slight lack of centro-symmetry is a graphical artifact.

The size of the counter-rotating region is remarkably uniform over the ribbon radii ρ and Reynolds numbers Re that we have studied. We define the streamwise extent of the counter-rotating region as delimited by $\psi(x, y = 0) = 0$, i.e. the x values at which the streamfunction at midheight $y = 0$ has the same value as at the channel walls $y = \pm 1$. For

$\rho = 0.086$, the counter-rotating region varies from $|x| \leq 2.18$ for $Re = 150$ to $|x| \leq 3.00$ for $Re = 300$, while for $\rho = 0.043$ the counter-rotating region varies from $|x| \leq 2.10$ for $Re = 150$ to $|x| \leq 2.87$ for $Re = 600$. This insensitivity to the size of ρ is significant in light of the 2D finite-amplitude steady states calculated by Cherhabili and Ehrenstein [8,9]. The states found by these authors in unperturbed plane Couette flow strongly resemble that in Fig. 3. These too have a central counter-rotating region surrounded by larger regions of negative circulation. At $Re = 2200$, the counter-rotating region in their flow occupies $|x| \leq 2.31$ (see Figs. 10 and 11 of [8], Figs. 2 and 3 of [9]) The similarity between the 2D flows for $\rho = 0.086$, $\rho = 0.043$, and, effectively, $\rho = 0$ leads us to hypothesize that our 2D perturbed plane Couette flows are connected (via the limit $\rho \to 0$) to those computed by Cherhabili and Ehrenstein.

We may also quantify the intensity of the counter-circulation. One measure is the maximum absolute value of v, which is attained very near the ribbon, at $(x, y) = (\pm 0.081, 0)$. This value is approximately independent of Reynolds number, but decreases strongly with ribbon radius: $v_{max} \approx 0.031$ for $\rho = 0.086$ and $v_{max} \approx 0.013$ for $\rho = 0.043$.

An important qualitative feature of the flow can been seen in Figs. 3(b) and (c): the flow is centro-symmetric, i.e. it is invariant under combined reflection in x and y, or equivalently rotation by angle π about the origin. It can be verified that the governing equations (1) and boundary conditions (2) are preserved by the centro-symmetric transformation:

$$\mathbf{u}(x, y) \to -\mathbf{u}(-x, -y). \tag{6}$$

The unperturbed plane Couette problem is also centro-symmetric. It is in fact symmetric under the Euclidean group E_1 of translations and the "reflection" consisting of the centro-symmetric transformation (6). The ribbon in the perturbed flow breaks the translation symmetry, but leaves the centro-symmetry intact. Note that reflections in x or y alone are not symmetries of either the unperturbed or the perturbed plane Couette problem because either reflection alone reverses the direction of the channel walls, violating the boundary conditions (2b).

In Fig. 4 we present streamwise velocity profiles near the ribbon. For $|x| > 0.5$, the Couette profile is very nearly recovered. Figure 4(b) shows streamwise velocity profiles of the deviation from the linear Couette profile across the full channel. Close examination reveals that these profiles are not odd in y, consistent with the fact that the system is neither symmetric nor antisymmetric under reflection in y. The symmetric partners to the profiles shown are at negative x values.

The profiles in Fig. 4 are similar to those Bottin et al. [4] obtained in the Saclay experiments under similar conditions. It is not possible to compare directly with experiment because of the difficulty in obtaining experimental velocity profiles and because the geometric perturbations differ in the computations and experiments. The only noticeable difference between experiments and computations is that the profiles Fig. 4(b) are very nearly odd in y, whereas in experiment this lack of symmetry is more pronounced.

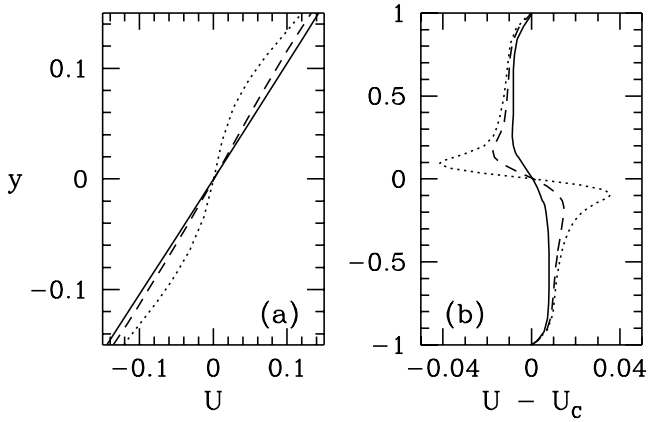

FIG. 4. Streamwise velocity profiles in the perturbed geometry. (a) $U(x, y)$ as a function of y for $x = 0.081$ (dotted), $x = 0.25$ (dashed), and $x = 0.5$ (solid). Only the central portion of the channel is shown. Only very close to the ribbon does the velocity differ significantly from the linear profile. (b) Deviation $U(x, y) - y$ over the full range of y.

Finally in Fig. 5 we quantify the deviation between perturbed and unperturbed plane Couette flow by plotting the energy per unit length $E \equiv \int_{-1}^{1} \frac{1}{2}|\mathbf{U}(x,y) - \mathbf{U}_{\rm C}(y)|^2 dy$ as a function of x for $-56 \leq x \leq 56$. The data show a narrow central region, corresponding to the region $|x| \leq 2.76$ of positive circulation seen in Fig. 3(b), where the deviation falls sharply and approximately exponentially in x. For $|x| > 2.76$, the deviation, while very small, decays very slowly (and not exponentially) with $|x|$. The boundaries $x = \pm 23.78$ terminating the outer region of negative circulation can also be seen on fig. 5. The precision of the computations is surpassed beyond $|x| = 40$. This figure shows that for $|x| > 32$ the deviation of the base flow from Couette is indeed very weak and this supports our choice of $L = 32$ as an adequate domain size for most computations.

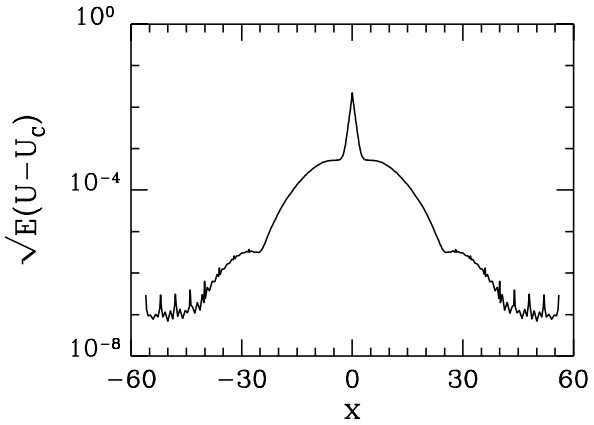

FIG. 5. Energy $\int_{-1}^{1} \frac{1}{2}|\mathbf{U}(x,y) - \mathbf{U}_{\rm C}|dy$ of deviation between perturbed and unperturbed Couette flows. Parameters are the same as in Fig. 3 except that here $L = 56$. Abrupt changes in slope at $|x| = 2.76, |x| = 23.78$ correspond to changes in the sign of the circulation of $\mathbf{U} - \mathbf{U}_{\rm C}$. For $|x| \gtrsim 40$, the deviation is below the precision of the computations.

B. Linear stability results

The two-dimensional steady flows just discussed become linearly unstable to three-dimensional perturbations when the Reynolds number exceeds a critical value Re_c. To determine this value and the associated wavenumber, we have performed a linear stability analysis of the steady flows via the procedure described in Sec. II B.

Figure 6 shows the growth rate σ of the most unstable three-dimensional eigenmode $\tilde{\mathbf{u}}$ as a function of Re and spanwise wavenumber β for a ribbon with $\rho = 0.086$. For each value of Re, we have fit a piecewise-cubic curve, shown in fig. 6, through the eigenvalue data to determine the wavenumber $\beta_{\max}(Re)$ which maximizes σ. The critical Reynolds number Re_c is then determined by linear interpolation of $\sigma(\beta_{\max}(Re), Re)$ through these maxima and finding its zero crossing. From this we find critical values for the onset of linear instability to be $Re_c = 230$ and $\beta_c = 1.3$ for the ribbon with $\rho = 0.086$. These values are consistent with what is seen experimentally, but we delay discussion until after the nonlinear stability is presented.

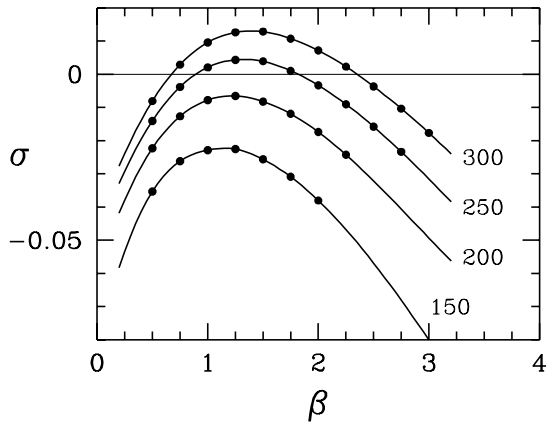

FIG. 6. Growth rate σ of most unstable three dimensional eigenmode as a function of spanwise wavenumber β for $Re = 150, 200, 250, 300$ with ribbon radius $\rho = 0.086$. Critical values for instability are $Re_c = 230$ and $\beta_c = 1.3$.

Figure 7 shows similar eigenvalue spectra for a ribbon half as large: $\rho = 0.043$. The critical wavenumber $\beta_c \approx 1.5$ is only slightly larger than the previous value. However, the critical Reynolds number is much larger: $Re_c \approx 550$. The critical Reynolds number must increase as ρ is decreased since, when no ribbon is present, the problem reduces to classical plane Couette flow which is linearly stable for all finite Re, i.e. $\lim_{\rho \to 0} Re_c(\rho) = \infty$.

We note that Cherhabili and Ehrenstein [9] also calculate 3D instability for their 2D finite amplitude plane Couette flows. Despite the resemblance of their 2D flows to ours, the spanwise wavenumber corresponding to maximal growth is much larger in their case: $\beta \approx 23$.

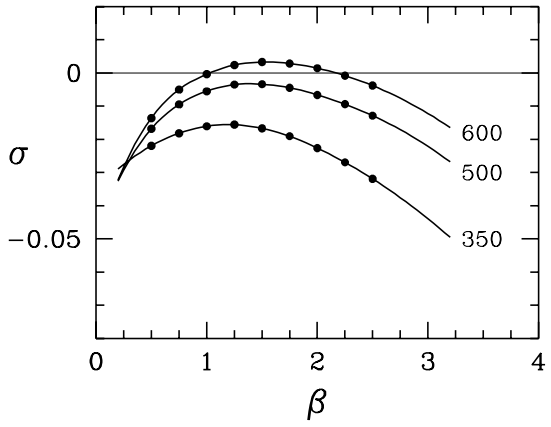

FIG. 7. Growth rate of most unstable eigenmode as a function of β and Re for $\rho = 0.043$. Critical values are $Re_c \approx 550$ and $\beta_c \approx 1.5$.

A computed eigenvector $\tilde{\mathbf{u}} = (\tilde{u}, \tilde{v}, \tilde{w})$ is shown in Figs. 8 and 9. This eigenvector is near-marginal: $Re = 250$, close to $Re_c = 230$. The spanwise wavelength is $\lambda = \lambda_c \equiv 2\pi/\beta_c = 4.83$. The other parameters are $\rho = 0.086$ and $L = 32$.

Figure 8 shows $(\tilde{v}, \tilde{w})$ velocity plots at four streamwise locations. In the $x = 0$ plane containing the ribbon, the flow is reflection-symmetric in y, and the flow is primarily spanwise. The trigonometric dependence in z with the choice of phase (3) can be seen. In the planes $x = 1$, $x = 2$, and $x = 3$, two counter-rotating streamwise vortices are present. The flow for negative x is obtained by reflection in y.

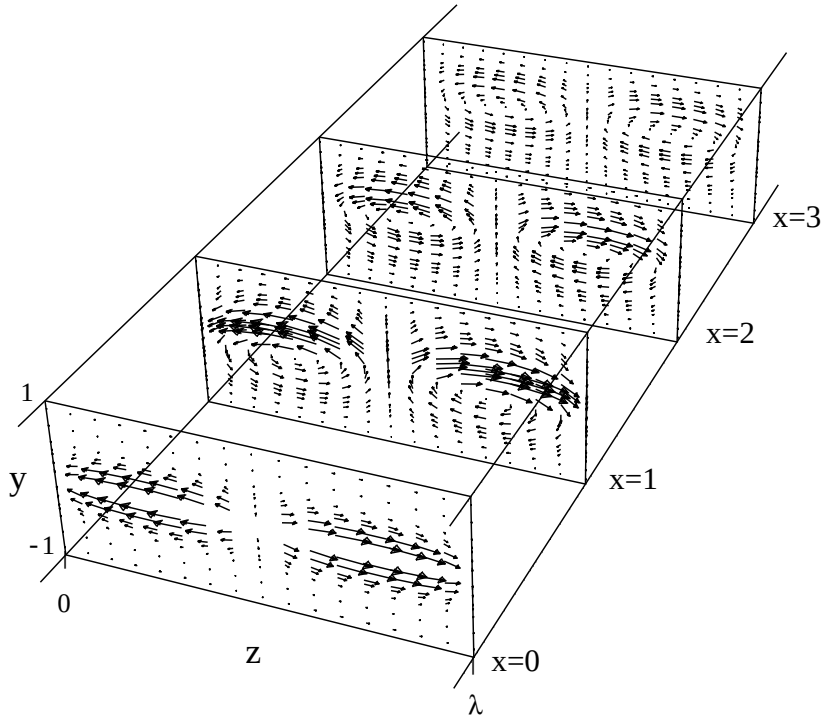

FIG. 8. Velocity field of near-marginal eigenvector in the planes $x = 0$, $x = 1$, $x = 2$, and $x = 3$. Parameters are $Re = 250$, $\rho = 0.086$, $L = 32$, $\lambda = 4.83$. At $x = 0$, the velocity is reflection-symmetric in y and primarily spanwise. The ribbon is seen as the area $|y| < \rho = 0.086$ with no flow. Streamwise vortices are visible for $x \geq 1$. The scale for distances in x is stretched by a factor of 3.333 relative to distances in y,z.

Figure 9 presents two complementary views of the eigenvector $\tilde{\mathbf{u}}$ for $-1 < x < 13$. Above is a plot of $(\tilde{u}, \tilde{v})$ in the plane $z = 0$ where they are maximal (cf. eq. 3). Below is a plot of $(\tilde{u}, \tilde{w})$ in the plane $y = 0$ at mid-channel height.

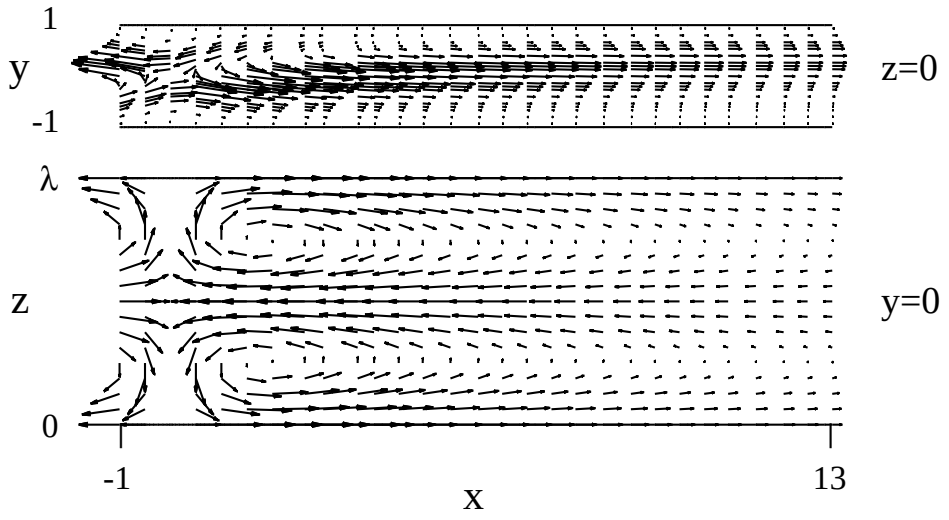

FIG. 9. Velocity field of near-marginal eigenvector in the planes $z = 0$ and $y = 0$.

Figure 10 shows the square root of energy per unit length $E \equiv \int_0^{\lambda_c} dz \int_{-1}^{+1} dy \ \frac{1}{2}|\tilde{\mathbf{u}}|^2$ as a function of x. Here, the eigenvector was computed in a larger domain ($L = 56$) in order determine its long-range behavior. The eigenvector is localized: the energy decays exponentially with $|x|$ and does not reflect the counter- and co- rotating regions of the 2D base flow seen on Fig. 5. The flow deficit due to the ribbon produces the local minimum at $x = 0$.

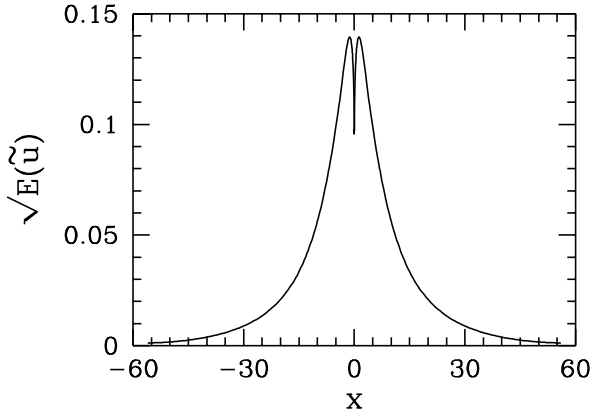

FIG. 10. Square root of energy per unit length in x of near-marginal eigenvector. Parameters are the same as in Figs. 8 and 9 except that here $L = 56$. Vertical scale is arbitrary.

We have also computed the vorticity of the eigenvector. Despite the streamwise vortices visible on Fig. 8, ω_x is the smallest vorticity component and ω_z by far the largest over most of the domain.

C. Nonlinear stability results

Our method of nonlinear stability analysis has previously been used to determine the nature of the bifurcation to three-dimensionality in the cylinder wake [24]. The method is based on tracking the nonlinear evolution of the 3D flow starting from an initial condition near the bifurcation at Re_c. "Near" refers both to phase space (i.e. a small 3D perturbation from the two-dimensional profile) and to parameter space (i.e. at a Reynolds number slightly above the linear instability threshold). In essence we follow the dynamics along the unstable manifold of the $2D$ steady flow far enough to determine how the nonlinear behavior deviates from linear evolution. From this we can determine very simply whether the instability is subcritical or supercritical.

Three-dimensional simulations are carried out at $Re = 250$, slightly above $Re_c = 230$, starting with an initial condition of the form:

$$\mathbf{u}(x, y, z) = \mathbf{U}(x, y) + \epsilon \tilde{\mathbf{u}}(x, y, z), \tag{7}$$

where $\mathbf{U}$ is the 2D base flow at $Re = 250$, $\tilde{\mathbf{u}}$ is its eigenmode at wavenumber $\beta_c = 1.3$, and ϵ is a small number controlling the size of the initial perturbation.

The restriction to wavenumbers which are multiples of β_c accurately captures the evolution from initial condition (7), since the Navier–Stokes equations preserve this subspace of 3D solutions. That is, we seek only to follow the evolution in the invariant subspace containing the critical eigenmode. We do not address the issue of whether the λ_c-periodic flow is itself unstable to long-wavelength perturbations.

To analyze the nonlinear evolution, we define the (real) amplitude A of the 3D flow as:

$$A \equiv \left[\frac{1}{2} \int_\Omega |\hat{\mathbf{u}}_1|^2 \, d\Omega \right]^{1/2}, \tag{8}$$

where Ω is the 2D cross-section of the computational domain and $\hat{\mathbf{u}}_1(x, y, t)$ is the Fourier component of the 3D velocity field at wavenumber β_c, i.e. the square root of the energy of the flow at wavenumber β_c. (A complex amplitude, not required here, would include the phase of the solution in the spanwise direction.)

Figure 11 shows the time evolution of A from our simulations. The value of ϵ is such that the initial energy of the 3D perturbation, $\epsilon\tilde{\mathbf{u}}$, is $E = A^2 = 8.35 \times 10^{-6}$; the energy of the base flow $\mathbf{U}$ is $E = 21.3$.

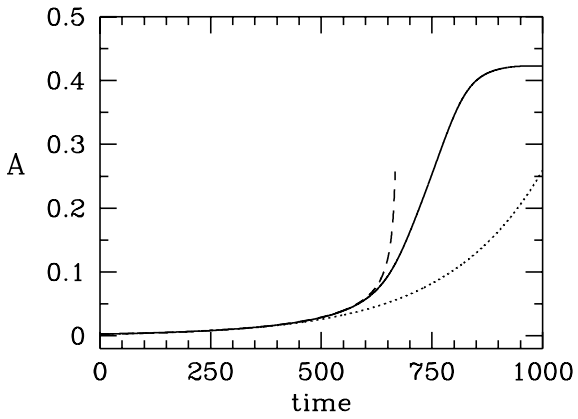

FIG. 11. Nonlinear growth of the amplitude A of the 3D flow from simulation (solid). First-order (dotted) and third-order (dashed) dynamics are shown with $\sigma = 0.0046$ and $\alpha = 1.4$. The faster than exponential nonlinear growth (i.e. positive α) shows that the instability at Re_c is subcritical.

To interpret the nonlinear evolution, consider the normal form for a pitchfork bifurcation including terms up to third-order in the amplitude:

$$\dot{A} = \sigma A + \alpha A^3 \tag{9}$$

The leading nonlinear term is cubic because the 3D bifurcation is of pitchfork type (an $O(2)$ symmetric pitchfork bifurcation). The Landau coefficient α determines the nonlinear character of the bifurcation. If $\alpha > 0$, then the nonlinearity is destabilizing at lowest order

and the bifurcation is subcritical; if $\alpha < 0$, then the cubic term saturates the instability and the bifurcation is supercritical.

Figure 11 includes curves for first-order evolution (i.e. $\dot{A} = \sigma A$) and the third-order evolution given by Eq. (9). For the first-order evolution, the eigenvalue σ for the bifurcation has been computed via the linear stability analysis in Sec. III B. For the third-order evolution we have simply fit the one remaining parameter, α, in the normal form. We find that $\alpha = 1.4 \pm 0.1$, and thus that the instability is subcritical. This value of α is essentially unchanged when the mesh is refined by increasing the polynomial order N to 10 or the number M of Fourier modes to 32. The nonlinear saturation seen in the time series is not captured by including a fifth-order term in the normal form. This means that the global structure of the nonlinear flow cannot be modeled by a single, low-order equation. We have additionally verified that the instability is subcritical by computing nonlinear states below Re_c (see below).

In Fig. 12, we show the 3D flow at $t = 1200$, the last point in our 3D simulations. This figure is analogous to fig. 8 depicting the eigenvector, so we will emphasize here the ways in which the two flows differ. Small streamwise vortices can be seen in each of the four corners of the $x = 0$ plane containing the ribbon. The lower ($y < 0$) pair evolve with x into the strong pair of vortices at $x = 1$. The vortices at $x = 3$ are tilted with respect to their counterparts in the eigenvector, attesting to the nonlinear generation of the second spanwise harmonic 2β. The 3D flow in the $y = 0$ and $z = 0$ planes (after subtraction of the dominant 2D base flow) is sufficiently similar to the eigenvector (fig. 9) that we do not present it here.

The streamwise velocity u of the 3D flow is shown in Fig. 13 and 14. Figure 13 shows equally spaced u-contours in the (y, z) plane at $x = 2$. Figure 14 shows streamwise velocity profiles $u(y)$ at the three x locations $x = 0$, $x = 1$, $x = 2$, and $x = 3$. At $z = 0$ (fig. 14(a)), u differs most from the 2D steady state and from plane Couette flow: u is approximately zero over the central half of the channel, with steeper gradients near the walls. Over most of the rest of the spanwise interval, u varies gradually between its boundary values of -1 and 1.

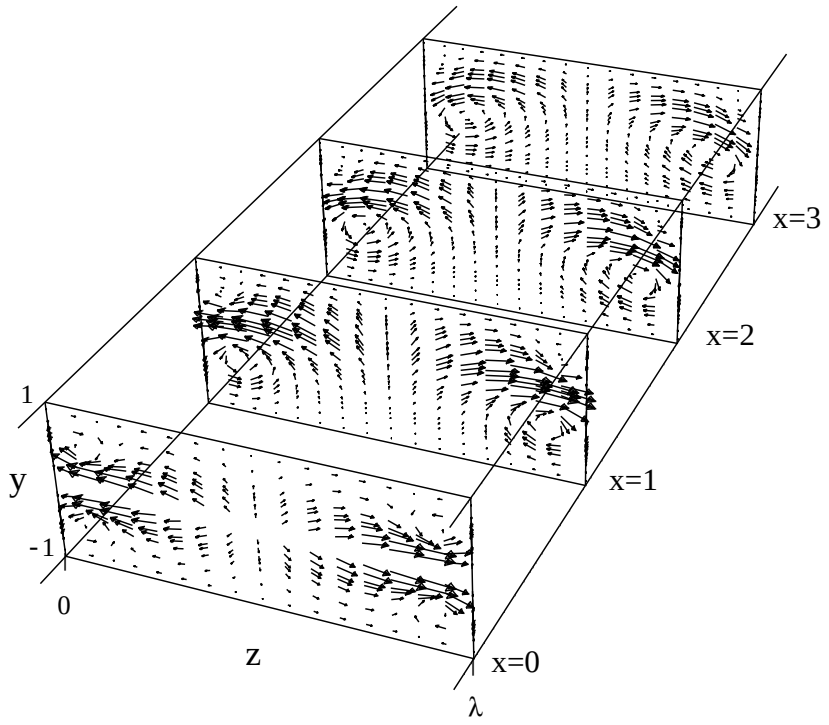

FIG. 12. 3D velocity field in the planes $x = 0$, $x = 1$, $x = 2$, and $x = 3$. Parameters are $Re = 250, \rho = 0.086, L = 32, \lambda = 4.83$. At $x = 0$, four small streamwise vortices can be seen in the corners of the domain. The lower ($y < 0$) vortex pair evolves into the large vortices seen at $x = 1$. The scale for distances in x is stretched by a factor of 3.333 relative to distances in y,z.

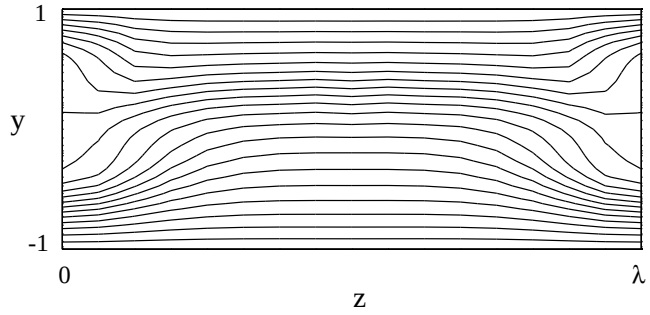

FIG. 13. Streamwise velocity contours in the plane $x = 2$ for the 3D field. u is small and nearly constant in the interior near $z = 0, \lambda$; elsewhere it varies approximately linearly with y.

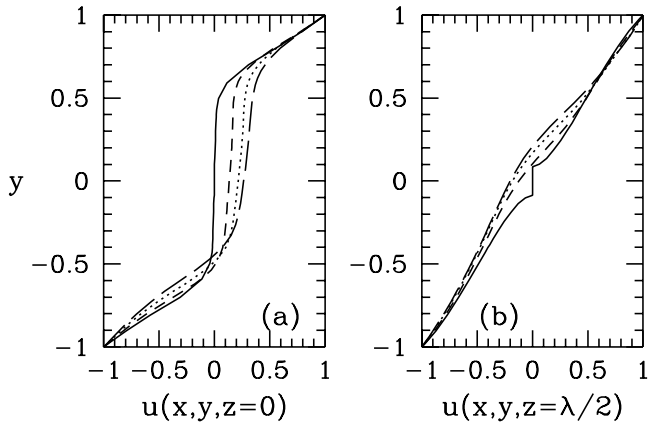

FIG. 14. Streamwise velocity profiles $u(y)$ for 3D field at $z = 0$, where the flow differs most from plane Couette flow, and at $z = \lambda/2$. Profiles are shown for $x = 0$ (solid), $x = 1$ (dashed), $x = 2$ (dotted), $x = 3$ (long-dashed).

The (v, w) projections of our 3D flow in Fig. 12, showing the tilted streamwise vortices, resemble the depictions of optimally growing modes by Butler and Farrell [10], of instantaneous turbulent flows by Hamilton et al. [15] and of weakly forced states by Coughlin [16]. However, our streamwise velocity u pictured in Fig. 13 differs significantly from [15,16] in that their u contours are much more strongly displaced at the vortex boundaries.

Far from the ribbon, the 3D flow returns to plane Couette flow. Figure 15 shows the dependence on x of the square root of energy per unit length of the deviation between the 3D flow and plane Couette flow: $E(\mathbf{U}-\mathbf{U}_C)(x) \equiv \int_{-1}^{+1} \frac{1}{2}|\mathbf{U}-\mathbf{U}_C|^2 dydz$. Note that the 3D flow is less localized than the corresponding eigenvector (Fig. 10). We have computed a 3D field at a lower Reynolds number, $Re = 200 < Re_c$, and a curve corresponding to this Reynolds value is also shown in Fig. 15. It can be seen that at the lower Reynolds number the deviation has lower energy, and importantly, occupies a smaller streamwise extent. This is in accord with the experimental observation that the streamwise extent of vortices in the perturbed flow decreases with decreasing Reynolds number.

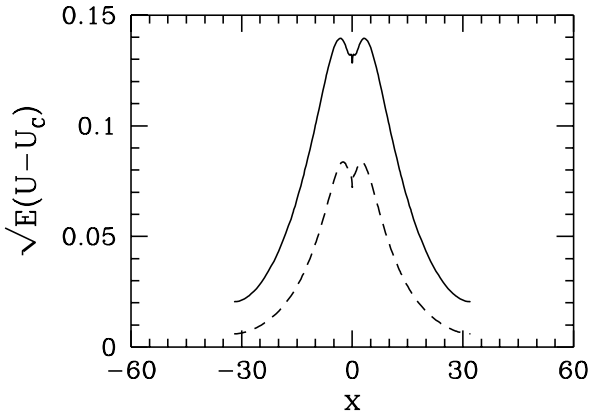

FIG. 15. Deviation from plane Couette flow of 3D velocity fields at $Re = 250$ (solid) and $Re = 200$ (dashed). Plotted is the square root of energy per unit length in x. The range in x is taken larger than the computational domain ($L = 32$) to match the range of Figs. 5 and 10.

IV. CONCLUSION

We have performed a computational linear and nonlinear stability analysis of perturbed plane Couette flow in order to understand features of, in particular, experiments recently performed at Saclay [2–4], and three-dimensional flows in the plane Couette system in general. We have accurately determined the extent to which the basic steady 2D profile is modified by the presence of a small spanwise-oriented ribbon in the flow. We have determined that such a ribbon, comparable in size to the cylinders used in the Saclay experiments, is large enough to induce linear instability of the basic profile at Reynolds numbers of order a few hundred. We have found that the spanwise wavelength of the most unstable mode is in good agreement with the value seen experimentally. Finally, we have shown that the linear instability produced by the ribbon is subcritical and leads to a flow with streamwise vortices. The streamwise extent occupied by these vortices decreases with decreasing Reynolds number as observed in experiment.

We elaborate further on how our analysis complements the Saclay experiments. In one set of experiments a fixed wire was placed in the flow and the 3D flows observed qualitatively and quantitatively as a function of Reynolds number. Specifically a bifurcation diagram was obtained [2,4] for the streamwise extent of the 3D flows as a function of Reynolds number for a wire of nondimensional radius 0.086. For Reynolds numbers in the range 160-300, coherent streamwise vortices were observed. In these experiments it was not determined whether the streamwise vortices first seen at $Re = 160$ arise from a linear instability of the 2D flow. Our results show that a small geometric perturbation does destabilize the 2D flow in a subcritical instability (at least for a ribbon of size $\rho = 0.086$) and that the bifurcating solution is a 3D flow with streamwise vortices of finite streamwise extent.

There are some minor differences between our results and the experimental findings that should be mentioned. The first is that 2D flows in our computations are more antisymmetric in the cross-channel direction y than in experiment (our Fig. 4 *vs.* Fig. 4 of [4]). This is probably due to the fact that we perturb our flow with an infinitely thin ribbon and not

a wire (cylinder) as in the experiment. However, based on the existence of instability in both cases, this small difference in the basic 2D flow is probably not very significant. The other difference between experiment and simulations arises because in our 3D simulations we impose spanwise periodicity with a single critical wavelength λ_c. Experimentally, it is observed that the streamwise vortices are not always regularly spaced in the spanwise direction and that at a certain critical Reynolds number (which depends on the wire radius) there is a transition to spatio-temporal intermittency. Neither of these effects are accessible to our confined simulations.

Future computational work is needed to explore these flows. It would be desirable to continue 2D and 3D solutions of the perturbed system to the plane Couette case, $\rho = 0$, and in particular, to connect the solutions we have found to those calculated by Cherhabili and Ehrenstein [8,9]. In addition, computations are needed to determine the spanwise wavelength of the 3D vortices selected nonlinearly in a domain of large spanwise extent, as well as the stability of these vortices.

ACKNOWLEDGMENTS

This research was in part conducted while the authors were visitors at the Institute for Mathematics and its Applications (IMA) of the University of Minnesota, which is supported by the National Science Foundation. We thank S. Bottin, O. Dauchot, and K. Coughlin for discussing their results with us prior to publication. We also thank A. Cherhabili, U. Ehrenstein, P. Manneville, and M. Rossi for stimulating discussions. We gratefully acknowledge R.D. Henderson for the use of *Prism*.

REFERENCES

[1] B.J. Bayly, S.A. Orszag, and T. Herbert, "Instability mechanisms in shear-flow transition," Annu. Rev. Fluid Mech., **20**, 359 (1988).

[2] O. Dauchot and F. Daviaud, "Streamwise vortices in plane Couette flow," Phys. Fluids **7**, 901 (1995).

[3] S. Bottin, O. Dauchot and F. Daviaud, "Intermittency in a locally forced plane Couette flow," Phys. Rev. Lett. **79**, 4377 (1997).

[4] S. Bottin, O. Dauchot, F. Daviaud, and P. Manneville, "Experimental evidence of streamwise vortices as finite amplitude solutions in transitional plane Couette flow," Phys. Fluids, submitted.

[5] M. Nagata, "Three-dimensional finite-amplitude solutions in plane Couette flow: bifurcation from infinity," J. Fluid Mech. **217**, 519 (1990).

[6] A.J. Conley and H.B. Keller, "Wavy Taylor vortices in plane Couette flow," preprint.

[7] R.M. Clever and F.H. Busse, "Three-dimensional convection in a horizontal fluid layer subjected to a constant shear," J. Fluid Mech. **234**, 511 (1992).

[8] A. Cherhabili and U. Ehrenstein "Spatially localized two-dimensional finite-amplitude states in plane Couette flow," Eur. J. Mech. B/Fluids **14**, 677 (1995).

[9] A. Cherhabili and U. Ehrenstein, "Finite-amplitude equilibrium states in plane Couette flow," J. Fluid Mech. **342**, 159 (1997).

[10] K.M. Butler and B.F. Farrell, "Three-dimensional optimal perturbations in viscous shear flow,", Phys. Fluids A **4**, 1637 (1992).

[11] S.C. Reddy and D.S. Henningson, "Energy growth in viscous channel flows," J. Fluid Mech. **252**, 209 (1993).

[12] L.N. Trefethen, A.E. Trefethen, S.C. Reddy, and T.A. Driscoll, "Hydrodynamic stability without eigenvalues," Science **261**, 578 (1993).

[13] S. A. Orszag and L.C. Kells, "Transition to turbulence in plane Poiseuille and plane Couette flow," J. Fluid Mech. **96**, 159 (1980).

[14] S.A. Orszag and A.T. Patera, "Subcritical transition to turbulence in plane channel flows," Phys. Rev. Lett. **45**, 989 (1980).

[15] J.M. Hamilton, J. Kim, and F. Waleffe, "Regeneration mechanisms of near-wall turbulence structures," J. Fluid Mech. **287**, 317 (1995).

[16] K. Coughlin, "Coherent structures and intermittent turbulence in channel flows. Part 1. Coherent structures," J. Fluid Mech., submitted.

[17] M. Nishioka, S. Iida, and J. Ichikawa, "An experimental investigation on the stability of plane Poiseuille flow," J. Fluid Mech. **72**, 731 (1975).

[18] M.F. Schatz, D. Barkley, and H.L. Swinney, "Instability in a spatially periodic open flow," Phys. Fluids **7**, 344 (1995).

[19] A.T. Patera, "A spectral element method for fluid dynamics; laminar flow in a channel expansion," J. Comput. Phys. **54**, 468 (1984).

[20] R.D. Henderson, "Unstructured spectral element methods; parallel algorithms and simulations," Ph.D. thesis, Princeton University, 1994.

[21] R.D. Henderson and G.E. Karniadakis, "Unstructured spectral element methods for simulation of turbulent flows," J. Comput. Phys. **122**, 191 (1995).

[22] G.E. Karniadakis, M. Israeli, and S.A. Orszag, "High-order splitting methods for the incompressible Navier-Stokes equations", J. Comput. Phys. **97**, 414 (1991).

[23] D. Barkley and R. Henderson, "Floquet stability analysis of the periodic wake of a circular cylinder," J. Fluid Mech. **322**, 215 (1996).

[24] R.D. Henderson and D. Barkley, "Secondary instability in the wake of a circular cylinder," Phys. Fluids **8**, 1683 (1996).

[25] C.K. Mamun and L.S. Tuckerman, "Asymmetry and Hopf bifurcation in spherical Couette flow," Phys. Fluids, **7**, 80 (1995).